Fabrication of Planar Heterojunction Perovskite Solar Cells by Controlled Low-Pressure Vapor Annealing

ARTICLE *in* JOURNAL OF PHYSICAL CHEMISTRY LETTERS · FEBRUARY 2015

Impact Factor: 7.46 · DOI: 10.1021/jz502720a

7 AUTHORS, INCLUDING:

Yanbo Li
Lawrence Berkeley National Laboratory
33 PUBLICATIONS **835** CITATIONS
SEE PROFILE

Raffaella Buonsanti
Lawrence Berkeley National Laboratory
55 PUBLICATIONS **1,578** CITATIONS
SEE PROFILE

Cinzia Giannini
Italian National Research Council
211 PUBLICATIONS **4,002** CITATIONS
SEE PROFILE

Francesca Maria Toma
Lawrence Berkeley National Laboratory
52 PUBLICATIONS **1,274** CITATIONS
SEE PROFILE

THE JOURNAL OF PHYSICAL CHEMISTRY Letters

Letter

pubs.acs.org/JPCL

Fabrication of Planar Heterojunction Perovskite Solar Cells by Controlled Low-Pressure Vapor Annealing

Yanbo Li,[†,‡] Jason K. Cooper,[†,‡] Raffaella Buonsanti,[†,‡] Cinzia Giannini,[§] Yi Liu,[∥] Francesca M. Toma,*[,†,⊥] and Ian D. Sharp*[,†,¶]

[†]Joint Center for Artificial Photosynthesis, Lawrence Berkeley National Laboratory, 1 Cyclotron Road, Berkeley, California 94720, United States

[‡]Materials Science Division, Lawrence Berkeley National Laboratory, 1 Cyclotron Road, Berkeley, California 94720, United States

[§]Institute of Crystallography, National Research Council, via Amendola 122/O, Bari 70126, Italy

[∥]The Molecular Foundry, Materials Science Division, Lawrence Berkeley National Laboratory, 1 Cyclotron Road, Berkeley, California 94720, United States

[⊥]Chemical Sciences Division, Lawrence Berkeley National Laboratory, 1 Cyclotron Road, Berkeley, California 94720, United States

[¶]Physical Biosciences Division, Lawrence Berkeley National Laboratory, 1 Cyclotron Road, Berkeley, California 94720, United States

Supporting Information

ABSTRACT: A new method for achieving high efficiency planar $CH_3NH_3I_{3-x}Cl_x$ perovskite photovoltaics, based on a low pressure, reduced temperature vapor annealing is demonstrated. Heterojunction devices based on this hybrid halide perovskite exhibit a top PCE of 16.8%, reduced $J-V$ hysteresis, and highly repeatable performance without need for a mesoporous or nanocrystalline metal oxide layer. Our findings demonstrate that large hysteresis is not an inherent feature of planar heterojunctions, and that efficient charge extraction can be achieved with uniform halide perovskite materials with desired composition. X-ray diffraction, valence band spectroscopy, and transient absorption measurements of these thin films reveal that structural modifications induced by chlorine clearly dominate over chemical and electronic doping effects, without affecting the Fermi level or photocarrier lifetime in the material.

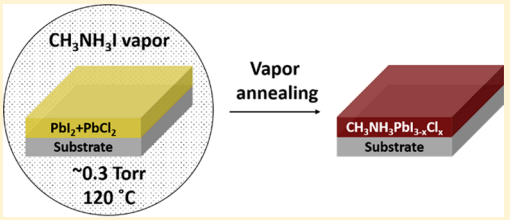

Hybrid organometal trihalide perovskites ($CH_3NH_3PbX_3$, X = I, Br, or Cl) have garnered significant attention in the last five years as highly promising semiconductors for thin film solar cells.[1−4] Impressive advancements in increasing the power conversion efficiency (PCE)—from approximately 4%[5] to over 19%[6]—have been achieved through optimization of the active layer fabrication process[7−10] and engineering of interfaces within photovoltaic devices.[11,12] State-of-the-art cells are based on either planar[13−17] or complex mesoporous/nanocrystalline[6,8−10,18] heterojunctions, which define the type of interface between the perovskite material and TiO_2.[19] Mesoporous and nanocrystalline TiO_2 electron selective contacts provide reduced carrier transport lengths and increased interfacial contact area, thereby facilitating efficient charge carrier collection and yielding the highest reported PCE values.[20] Although planar heterojunctions are desirable to provide simple and scalable cell configurations, as well as a more straightforward system for understanding device physics,[19,21] these materials typically yield relatively low power conversion efficiencies and large hysteresis in current−voltage characteristics.

A few attempts have been made to fabricate planar heterojunctions based on perovskite layers with improved homogeneity. For example, Snaith and collaborators reported the preparation of a uniform mixed perovskite ($CH_3NH_3PbI_{3-x}Cl_x$) layer through a dual-source evaporation process, with PCE values as high as 15.4%.[22] Although this work represents a significant advancement on the path to high efficiency planar devices, it requires high vacuum deposition in a dedicated system. Furthermore, open questions remain about the role of chloride in improving device efficiency. In an alternate process, Yang and collaborators demonstrated the fabrication of $CH_3NH_3PbI_3$ via the vapor-assisted solution process (VASP) by annealing lead iodide (PbI_2) films deposited on TiO_2/FTO in the presence of methylammonium iodide (CH_3NH_3I) at 150 °C under nitrogen atmosphere in a glovebox.[23] Although the perovskite layers prepared by this method exhibited extremely high uniformity, these films yielded relatively low (12.1%) device efficiency. Indeed, the thermal processing window of VASP is restricted to relatively high temperature compared to solution processed and thermally evaporated films due to the low vapor pressure of CH_3NH_3I, suggesting the need for additional process versatility and control.

Herein, we present a two-step low pressure VASP (LP-VASP) for the fabrication of pinhole-free, continuous perov-

Received: December 24, 2014
Accepted: January 16, 2015

DOI: 10.1021/jz502720a
J. Phys. Chem. Lett. 2015, 6, 493−499

skite layers for high efficiency thin film photovoltaics. In the first step, spin-coated mixed lead halide ($PbI_2/PbCl_2$) films provide homogeneous coverage of the planar substrate, as well as a chloride source. In the second step, samples are converted to the desired halide perovskite phase by simultaneous annealing and exposure to CH_3NH_3I vapor at low pressure (Scheme 1 and details in Supporting Information). For

Scheme 1. Schematic Representation of the Low Pressure Vapor Assisted Solution Process, LP-VASP, Reported Here[A]

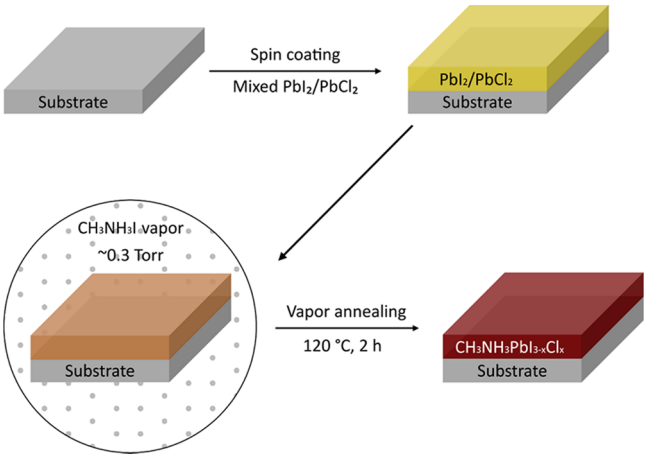

[A]Use of mixed halide precursors in the first step and the reduced temperature in the second step, which is enabled by the low pressure, provides the process versatility required for achieving the highest efficiency planar heterojunction solar cells. The substrate is FTO-coated glass with a 75 nm dense layer of TiO_2 deposited by electron-beam deposition.

comparison with films derived from mixed $PbI_2/PbCl_2$ precursors, pure iodide $CH_3NH_3PbI_3$ perovskite films with the same thickness were also synthesized by spin coating of pure PbI_2 precursor in the first reaction step, followed by processing under otherwise identical conditions.

Low pressure vapor annealing increases the vapor pressure of CH_3NH_3I, which enables the annealing temperature (120 °C) to be reduced with respect to VASP (150 °C).[23] The ability to access a broader range of synthesis temperatures, which is enabled by the reduced pressure, allows formation of thin films with structures that are correlated with improved device efficiency and reduced current−voltage hysteresis. Planar heterojunction solar cells fabricated by LP-VASP exhibit record power conversion efficiencies for this class of device, with a top efficiency of 16.8% and average efficiency of 15.7 ± 0.7% in the reverse scan direction. Importantly, current−voltage curves of these planar devices exhibit significantly reduced hysteresis compared to previously reported planar devices, with a top efficiency of 15.4% and average efficiency of 14.7 ± 0.7% measured in the forward scan direction.[6,24,25] We find that the presence of chloride during synthesis improves power conversion efficiency but does not have a measurable impact on bandgap, Fermi level position, or photocarrier lifetimes in our films. These results suggest that the dominant role of mixed halide precursors and reduced temperature in LP-VASP is to reduce texture toward thin films possessing randomized grain orientations, as described below.

Although chlorine is reported to greatly improve the transport properties in perovskite-based devices,[26] the mechanism by which it does so remains an open question. However, its incorporation to form a continuous solid phase, without segregation between $CH_3NH_3PbI_3$ and $CH_3NH_3PbCl_3$, is allowed only at low concentrations (<4%),[16,20] and it has been recently classified as a dopant agent.[8,27] Furthermore, elemental analysis of Cl in this material, particularly at low concentrations, is experimentally challenging. In the present work, X-ray photoelectron spectroscopy (XPS) showed no detectable chlorine in the near-surface region of films produced from mixed lead halide precursor. Bulk elemental analysis by X-ray fluorescence (XRF) spectroscopy showed no detectable chlorine, but sensitivity was limited by overlap of the Cl signal with Pb-related features. Nevertheless, these findings reveal that the chloride content is significantly reduced relative to the precursor ratio. If any chloride is present in the films, it is at low concentrations, consistent with previous reports of material deposited using other methods.[28−31]

Cross-sectional scanning electron microscopy (SEM) is used to assess film quality and determine morphology at each stage of synthesis (Figure 1a−b). Starting from a lead halide film thickness of ∼280 ± 20 nm, the low pressure vapor annealing process leads to a final perovskite layer that is ∼350 ± 30 nm thick, in agreement with previously reported expansion of the lead halide layer upon intercalation of CH_3NH_3I and conversion to perovskite phase. Top view SEM images reveal the change in morphology associated with transformation to the perovskite phase, with final grain size of approximately 500 ± 100 nm (Figure 1c−d). Although grain boundaries in this materials system have been found to be surprisingly inert electronically, the presence of large grain sizes is expected to promote improved charge extraction efficiency. Importantly, the films are homogeneous and continuous over large areas, with no indications of pinhole defects that would adversely affect device performance (Figure S1, Supporting Information). Corresponding images for pure PbI_2 and $CH_3NH_3PbI_3$ thin films are reported in the Supporting Information (Figure S2, Supporting Information), and show similar homogeneity over large areas.

X-ray diffraction (XRD) of $CH_3NH_3PbI_{3-x}Cl_x$ and $CH_3NH_3PbI_3$ films produced at 120 °C provides evidence for the highly crystalline nature of our samples and show the tetragonal perovskite pattern with peaks at 14.12°, 28.44°, 31.88°, 43.18°, corresponding to (110), (220), (310), and (330), respectively (Figure 1e), similar to material produced via other methods.[23,32] No apparent shift of the XRD peaks is observed between the $CH_3NH_3PbI_{3-x}Cl_x$ and $CH_3NH_3PbI_3$, which is consistent with the low Cl content in the mixed halide films.[33] However, the relative intensity ratio of the (220) and (310) reflections is modified in the presence of chlorine. Analysis by Rietveld refinement (see Supporting Information) reveals significantly reduced texture in $CH_3NH_3PbI_{3-x}Cl_x$ films compared to $CH_3NH_3PbI_3$ films synthesized under identical conditions of LP-VASP (Supporting Information Figure S3). Interestingly, the XRD pattern of the $PbI_2/PbCl_2$ precursor shows peaks at 21.34°, 28.96°, 29.8°, 30.66°, 34.08°, corresponding to (120), (121), (130), (211), and (310) planes of PbICl phase, in addition to the expected PbI_2 phase (Figure S4, Supporting Information).[34] Kirmayer and collaborators have proposed that the nucleation step, which is determined by the presence of different precursor seeds, affects the morphology of perovskite polycrystalline films, and specifically $PbCl_2$ has been shown to provide a heterogeneous nucleation site for the formation of perovskite crystals in solution.[33] The simultaneous presence of different precursor seeds in the mixed

DOI: 10.1021/jz502720a
J. Phys. Chem. Lett. 2015, 6, 493−499

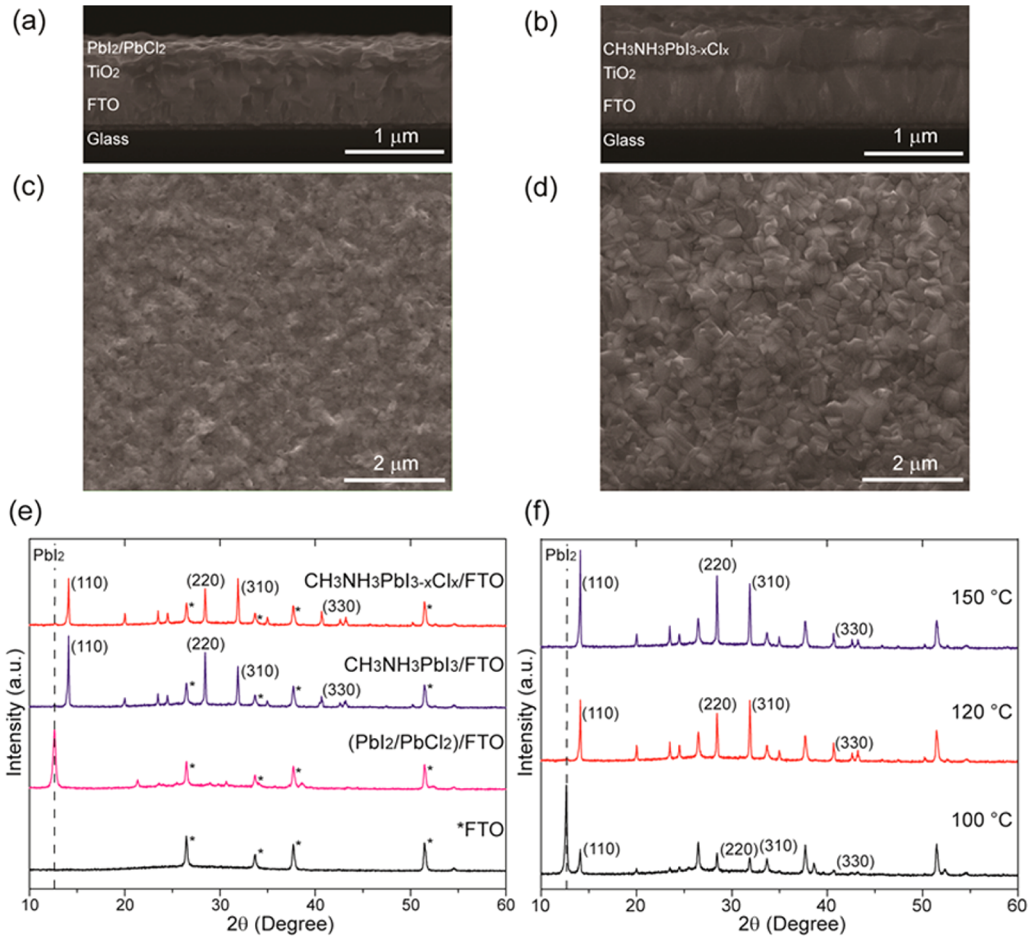

Figure 1. (a–b) Cross section and (c–d) top view scanning electron microscopy (SEM) images of (a,c) mixed lead halide and (b,d) Cl-doped metal organic lead halide perovskite layers. (e) X-ray diffraction (XRD) patterns of fluorine-doped tin oxide (FTO, black curve), mixed lead halide on FTO ($(PbI_2/PbCl_2)$/FTO, magenta curve), metal organic halide perovskite ($CH_3NH_3PbI_3$, blue curve), and doped metal organic halide perovskite ($CH_3NH_3PbI_{3-x}Cl_x$, red curve). (f) XRD patterns of $CH_3NH_3PbI_{3-x}Cl_x$ perovskite layers annealed at different temperature.

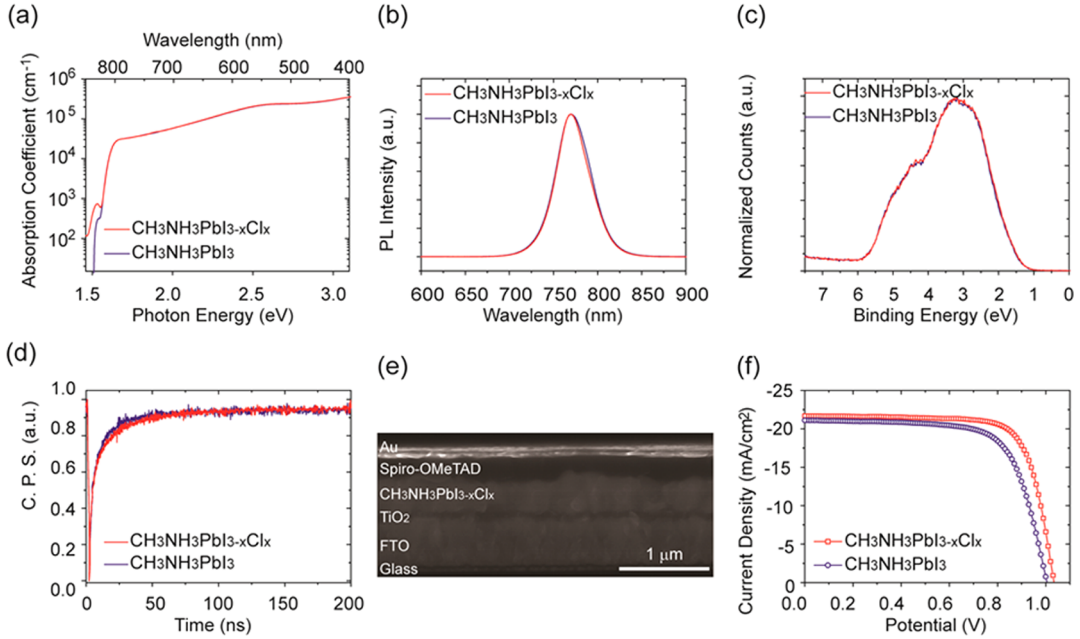

Figure 2. (a) Absorption, (b) photoluminescence, (c) valence band, and (d) transient absorption spectra of $CH_3NH_3PbI_3$ (blue curve), and $CH_3NH_3PbI_{3-x}Cl_x$ (red curve), (e) cross section SEM image of planar device architecture, and (f) current density (J)–voltage (V) curves of $CH_3NH_3PbI_3$ (blue curve) and $CH_3NH_3PbI_{3-x}Cl_x$ (red curve) based solar cells.

DOI: 10.1021/jz502720a
J. Phys. Chem. Lett. 2015, 6, 493–499

Table 1. Device Performance of Perovskite Solar Cells

	reverse scan				forward scan			
	J_{sc} (mA/cm^2)	V_{oc} (V)	FF	PCE (%)	J_{sc} (mA/cm^2)	V_{oc} (V)	FF	PCE (%)
$CH_3NH_3PbI_3$ (best)	21.1	1.00	0.70	14.8	21.2	0.97	0.66	13.6
$CH_3NH_3PbI_3$ (average)[a]	20.9 ± 0.4	1.00 ± 0.01	0.68 ± 0.01	14.2 ± 0.3	21.0 ± 0.5	0.96 ± 0.01	0.65 ± 0.01	13.1 ± 0.2
$CH_3NH_3PbI_{3-x}Cl_x$ (best)	21.7	1.04	0.75	16.8	21.7	1.01	0.70	15.4
$CH_3NH_3PbI_{3-x}Cl_x$ (average)[b]	21.3 ± 0.6	1.00 ± 0.02	0.73 ± 0.02	15.7 ± 0.7	21.3 ± 0.7	0.95 ± 0.02	0.69 ± 0.02	14.7 ± 0.7

[a]Standard deviation calculated on 8 devices. [b]Standard deviation calculated on 32 devices.

halides may also be responsible for the lack of preferential orientation of grains in the $CH_3NH_3PbI_{3-x}Cl_x$ compared to $CH_3NH_3PbI_3$.

By varying the temperature of our process, we have found that at low annealing temperature (100 °C), the conversion of the lead precursor into the perovskite material was largely incomplete. An intense peak at 12.66°, which is associated with the $PbI_2/PbCl_2$ film, is visible in the XRD pattern (Figure 1f, dashed vertical line). On the other hand, at high annealing temperature (150 °C), the lead halide film is fully converted into the perovskite material, with no residual PbI_2 peak in the XRD pattern. Annealing at 120 °C results in majority conversion of the film to the active perovskite phase and retention of a small fraction of PbI_2, as revealed by the small peak at 12.66°. Although this peak indicates incomplete conversion of the $PbI_2/PbCl_2$ film to active perovskite phase, the presence of residual PbI_2 has been found to be beneficial for device performance,[22,23] likely due to passivation of surface and grain boundary states.[35] Conventional VASP also allows PbI_2 passivation by variation of processing time. However, the ability to reduce processing temperature to simultaneously affect the crystallographic texture and incorporate PbI_2 using LP-VASP differentiates this method from the atmospheric pressure analogue. This process offers the opportunity to tune the chemical potential during the perovskite layer synthesis, which may have important effect on point defect formation and structural modification.[36] As will be discussed below, the highest device performance is achieved at the intermediate temperature and, unless otherwise noted, all data reported herein were obtained from films processed at 120 °C.

The absorption and photoluminescence properties of the synthesized $CH_3NH_3PbI_3$ and $CH_3NH_3PbI_{3-x}Cl_x$ perovskite thin films display similar characteristics (Figure 2a and b). The onset of the absorption is at ∼790 nm (∼1.6 eV), in agreement with previous measurements,[37] and the optical density continuously increases from ∼750 nm (1.7 eV) to 470 nm (2.6 eV, maximum). The optical band gap is calculated by analysis of the Tauc plots for direct band gap materials (Figure S5, Supporting Information) and is similar for the two compositions, with a value of ∼1.6 eV. Photoluminescence spectra show a strong emission at 773 nm.[38] The similarity of optical properties observed for the $CH_3NH_3PbI_3$ and $CH_3NH_3PbI_{3-x}Cl_x$ films is consistent with low concentration of Cl in the mixed halide film. Valence band spectroscopy was performed to investigate the role of chlorine on electronic doping of our films. As shown in Figure 2c, the valence band position for both classes of material are identical and are consistent with majority n-type character. Because the bandgaps of both $CH_3NH_3PbI_3$ and $CH_3NH_3PbI_{3-x}Cl_x$ are the same, we conclude that the presence of chlorine in the precursor does not have a significant impact on doping or Fermi level position. Furthermore, transient absorption measurements, shown in Figure 2d, reveal nearly identical photocarrier lifetimes (∼20 ns), which are also not significantly impacted by the presence or absence of chlorine during LP-VASP. These lifetimes are on the order of those commonly observed for films of pure iodide perovskites.[26,39] We note that a variety of reports have suggested that Cl enables long photocarrier lifetimes and increased diffusion lengths in halide perovskite materials.[26,39] Although such an effect impacts device performance for those synthetic approaches, it does not appear to be a dominant factor for LP-VASP.

Planar photovoltaic device architectures with dense, e-beam deposited TiO_2 as electron transport layer, $CH_3NH_3PbI_{3-x}Cl_x$ as active absorber layer, spiro-OMeTAD as hole transport layer, and Au as top contact were fabricated and used to evaluate performance (Figure 2e) under simulated air mass 1.5 global (AM 1.5G) illumination (100 mW/cm^2). Current density (J)−voltage (V) characteristic of our top performing devices based on $CH_3NH_3PbI_{3-x}Cl_x$ and undoped $CH_3NH_3PbI_3$ are reported in Figure 2f, and average performance, together with standard deviation of measurements of multiple devices, is summarized in Table 1.

The best mixed halide $CH_3NH_3PbI_{3-x}Cl_x$ perovskite solar cell is characterized by a short circuit current (J_{sc}) of 21.7 mA/cm^2, an open circuit voltage (V_{oc}) of 1.04 V, a fill factor (FF) of 0.75, and a PCE value of 16.8%. To the best of our knowledge, this device exhibits the highest reported efficiency for the planar perovskite/TiO_2 heterojunction architecture, including one of the highest fill factors, which is indicative of efficient charge extraction in our device without the need of a mesoporous TiO_2 scaffold or specific interface engineering. Interestingly, even the pure halide $CH_3NH_3PbI_3$ devices achieve high performance, with the best performing device providing a J_{sc} of 21.1 mA/cm^2, a V_{oc} of 1.00 V, a FF of 0.70, and a PCE of 14.8%. This finding suggests that the $CH_3NH_3PbI_3$ film (thickness: ∼350 nm) produced by LP-VASP has much higher charge extraction efficiency than films produced by conventional spin coating method.[26] The average efficiency is 15.7 ± 0.7% and 14.2 ± 0.3% for $CH_3NH_3PbI_{3-x}Cl_x$ and $CH_3NH_3PbI_3$, respectively (Table 1, and Figure S6 in Supporting Information), thereby proving the high reproducibility of our synthetic method.

As described above, we have also investigated the role of processing temperature on formation of perovskite layers and the impact on device performance. For films processed at 100 °C, incomplete conversion to perovskite, characterized by excess of PbI_2 in the active layer, has a detrimental effect on device efficiencies, with PCEs lower than 4% (Figure S7, Supporting Information). At a higher annealing temperature (150 °C), no residual PbI_2 is observed but the efficiency is only 12.1% (Figure S7, Supporting Information), which correlates well with the one reported by Yang and co-workers at the same temperature. In the present work, the highest efficiency devices are made with films annealed at 120 °C, which always show a small PbI_2 peak in the XRD pattern. In addition, it is worth

DOI: 10.1021/jz502720a
J. Phys. Chem. Lett. 2015, 6, 493−499

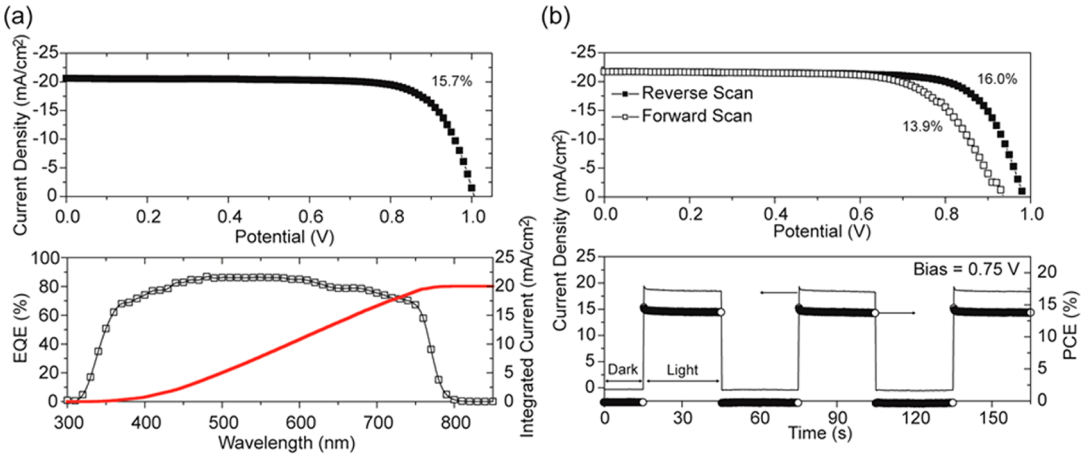

Figure 3. (a) $J-V$ curve (top) and external quantum efficiency (EQE, black curve with empty squares, bottom) with integrated current (red curve, bottom) of a typical $CH_3NH_3PbI_{3-x}Cl_x$ solar cell, and (b) reverse (filled square) and forward (empty square) scan $J-V$ curves (top) and photocurrent density (left axis) and PCE values (right axis) of a typical $CH_3NH_3PbI_{3-x}Cl_x$ device measured under dark and under illumination as a function of time at 0.75 V (bottom).

noting that the $CH_3NH_3PbI_{3-x}Cl_x$ film annealed at 150 °C, as well as the undoped sample, are characterized by more thin film texture, whereas the Cl-doped sample annealed at 120 °C presents almost random grain orientation (Supporting Information Figure S3). The above results suggest that moderate annealing temperature, enabled by low pressure, is of fundamental importance for achieving high efficiency devices. The observation that chlorine does not affect electronic doping or photocarrier lifetimes in our films, together with reduced texture observed in the $CH_3NH_3PbI_{3-x}Cl_x$ films, further suggest that structural modifications induced by the presence of chloride dominate over a chemical or electronic doping effects. Our observations are consistent with a recent study from Petrozza and co-workers, in which they demonstrated that chlorine ions, even if not in a detectable concentration, drive the crystallization dynamics, impact the crystalline order, and affect the crystallographic orientation of grains for the case of films deposited by spin-coating.[40] Dar and co-workers also demonstrated that the presence of Cl ions in the precursor influence the growth of $CH_3NH_3PbI_3$ significantly without occupying the lattice.[29] Charge transport and extraction in the out-of-plane direction is likely to be affected by anisotropy in the material, as suggested by Bein and collaborators.[41]

The photovoltaic characteristics of typical $CH_3NH_3PbI_{3-x}Cl_x$ devices are reported in Figure 3. Figure 3a shows the $J-V$ curve and the corresponding external quantum efficiency (EQE) spectrum of a typical device with a PCE of 15.7%. In the EQE spectrum, the onset of the photocurrent is at ∼790 nm, which is in agreement with the absorption spectrum as well as with the measured band gap of this material (Figure 2a, and Figure S5, Supporting Information). Our perovskite layer provides efficient charge extraction over a large part of the visible spectrum (370−650 nm), with a maximum EQE of ∼86% measured between 460 and 630 nm. The integrated photocurrent is 20 mA/cm^2 (Figure 3b), within 3% of the measured J_{SC} of the device (Figure 3a). Dark $J-V$ characteristics of these solar cells are provided in Supporting Information Figure S8 and exhibit similar characteristics to those previously reported.[42]

Despite the great promise of hybrid halide perovskites for photovoltaic applications, recent work has pointed to a significant hysteresis in current−voltage curves.[20,24,25] In detail, when the device is scanned in the reverse bias direction (from V_{oc} to J_{sc}), the performance metrics are higher than when it is scanned in the forward bias direction (from J_{sc} to V_{oc}). Although the specific origin of this hysteresis remains unknown, it is particularly pronounced for the case of planar device architectures and this issue represents one of the major challenges to further improve perovskite efficiency for steady state operation and large-scale application. In order to evaluate the hysteretic behavior of our devices (Figure 3b), $J-V$ curves were recorded every 10 mV at a scan rate of ∼0.5 V s^{-1} in both scan directions, and differences between forward and reverse scan PCE values are generally less than 2% for both the pure and mixed halide devices based on materials synthesized with our method (Table 1). Hysteretic behavior of these devices was consistent over repeated measurements under illumination (Figure S9, Supporting Information), and also had a similar magnitude in forward and reverse dark scans (Figure S10, Supporting Information). In addition, current density and PCE values have been studied as a function of time at a constant forward bias of 0.75 V in order to establish the steady state performance and probe potential transient characteristics upon illumination (Figure 3b). After an initial drop, which settles to a constant value in approximately 1 s, these outputs display a remarkable stability over time with a current density of approximately 18.5 mA/cm^2 and PCE of about 14.0%. Reverse versus forward bias scans and steady-state current measurements show that $CH_3NH_3PbI_{3-x}Cl_x$ based devices are characterized by minimal hysteresis compared to planar geometry reported in literature and studied under similar conditions.[6,24,25] Similarly, small hysteresis has been observed for the undoped device (Figure S11, Supporting Information).

Our findings using LP-VASP demonstrate that large hysteresis is not an inherent feature of planar heterojunctions and that efficient charge extraction can be achieved with material possessing uniform coverage and desired structure. Therefore, our method provides a route to high efficiency planar photovoltaic cells exhibiting small hysteresis. Integration of our synthetic process with mesoporous architectures, as well as interface engineering, has potential to further increase efficiency and reduce hysteresis.

DOI: 10.1021/jz502720a
J. Phys. Chem. Lett. 2015, 6, 493−499

In conclusion, we have developed LP-VASP, a versatile method for the synthesis of homogeneous, pinhole-free, halide perovskite thin films. This process is based on in situ annealing of a thin layer of lead halide precursor in the presence of CH_3NH_3I at low pressure in order to achieve controlled intercalation at reduced temperature. Physical characterization of halide perovskite films produced by our method reveals that low temperature processing in the presence of Cl reduces texture in perovskite thin films while also enabling retention of a minor secondary phase of lead iodide, which is important for improved device performance. Within experimental sensitivity, we do not detect chlorine in the synthesized films. Furthermore, the bandgap, Fermi level, and photocarrier lifetime are not significantly affected by the presence of chlorine during synthesis. These results suggest that the dominant impact of mixed halide precursors is structural, rather than chemical or electronic, in nature. Planar photovoltaic devices based on this material exhibit exceptional power conversion efficiency, of up to 16.8%, and minimal hysteresis, of less than 2%, compared to existing halide perovskite solar cells based on similar architecture. Thus, this process enables highly repeatable devices, which possess the highest reported efficiency and lowest hysteresis for planar systems of this architecture.

■ ASSOCIATED CONTENT

Supporting Information

Experimental details on solar cell fabrication and supporting characterization are reported in the Supporting Information. This material is available free of charge via the Internet at http://pubs.acs.org.

■ AUTHOR INFORMATION

Corresponding Authors

*E-mail: fmtoma@lbl.gov.
*E-mail: idsharp@lbl.gov.

Notes

The authors declare no competing financial interest.

■ ACKNOWLEDGMENTS

This material is based upon work performed by the Joint Center for Artificial Photosynthesis, DOE Energy Innovation Hub, supported through the Office of Science of the U.S. Department of Energy under Award Number DE-SC0004993. Photovoltaic characterization was performed at the Molecular Foundry, which is supported by the U.S. Department of Energy (DOE), Office of Basic Energy Sciences, Scientific User Facilities Division, under Contract No. DE-AC02-05CH11231. We gratefully acknowledge Dan Guevarra and Joel A. Haber of the Joint Center for Artificial Photosynthesis, California Institute of Technology, for providing elemental analysis of thin film samples by X-ray fluorescence spectroscopy, and Teresa L. Chen from the Molecular Foundry for help with PV measurements.

■ REFERENCES

(1) Green, M. A.; Ho-Baillie, A.; Snaith, H. J. The Emergence of Perovskite Solar Cells. *Nat. Photonics* **2014**, *8*, 506−514.
(2) Gao, P.; Gratzel, M.; Nazeeruddin, M. K. Organohalide Lead Perovskites for Photovoltaic Applications. *Ener. Environ. Sci.* **2014**, *7*, 2448−2463.
(3) Snaith, H. J. Perovskites: The Emergence of a New Era for Low-Cost, High-Efficiency Solar Cells. *J. Phys. Chem. Lett.* **2013**, *4*, 3623−3630.
(4) Kazim, S.; Nazeeruddin, M. K.; Grätzel, M.; Ahmad, S. Perovskite As Light Harvester: A Game Changer in Photovoltaics. *Angew. Chem., Int. Ed.* **2014**, *53*, 2812−2824.
(5) Kojima, A.; Teshima, K.; Shirai, Y.; Miyasaka, T. Organometal Halide Perovskites As Visible-Light Sensitizers for Photovoltaic Cells. *J. Am. Chem. Soc.* **2009**, *131*, 6050−6051.
(6) Zhou, H.; et al. Interface Engineering of Highly Efficient Perovskite Solar Cells. *Science* **2014**, *345*, 542−546.
(7) Im, J.-H.; Lee, C.-R.; Lee, J.-W.; Park, S.-W.; Park, N.-G. 6.5% Efficient Perovskite Quantum-Dot-Sensitized Solar Cell. *Nanoscale* **2011**, *3*, 4088−4093.
(8) Kim, H.-S.; et al. Lead Iodide Perovskite Sensitized All-Solid-State Submicron Thin Film Mesoscopic Solar Cell with Efficiency Exceeding 9%. *Sci. Rep.* **2012**, *2*, 591.
(9) Lee, M. M.; Teuscher, J.; Miyasaka, T.; Murakami, T. N.; Snaith, H. J. Efficient Hybrid Solar Cells Based on Meso-Superstructured Organometal Halide Perovskites. *Science* **2012**, *338*, 643−647.
(10) Burschka, J.; Pellet, N.; Moon, S.-J.; Humphry-Baker, R.; Gao, P.; Nazeeruddin, M. K.; Gratzel, M. Sequential Deposition As a Route to High-Performance Perovskite-Sensitized Solar Cells. *Nature* **2013**, *499*, 316−319.
(11) Jeon, N. J.; Noh, J. H.; Kim, Y. C.; Yang, W. S.; Ryu, S.; Seok, S. I. Solvent Engineering for High-Performance Inorganic−Organic Hybrid Perovskite Solar Cells. *Nat. Mater.* **2014**, *13*, 897−903.
(12) Liang, P.-W.; Liao, C.-Y.; Chueh, C.-C.; Zuo, F.; Williams, S. T.; Xin, X.-K.; Lin, J.; Jen, A. K. Y. Additive Enhanced Crystallization of Solution-Processed Perovskite for Highly Efficient Planar-Heterojunction Solar Cells. *Adv. Mater.* **2014**, *26*, 3748−3754.
(13) Chen, C.-W.; Kang, H.-W.; Hsiao, S.-Y.; Yang, P.-F.; Chiang, K.-M.; Lin, H.-W. Efficient and Uniform Planar-Type Perovskite Solar Cells by Simple Sequential Vacuum Deposition. *Adv. Mater.* **2014**, *26*, 6647−6652.
(14) Eperon, G. E.; Burlakov, V. M.; Docampo, P.; Goriely, A.; Snaith, H. J. Morphological Control for High Performance, Solution-Processed Planar Heterojunction Perovskite Solar Cells. *Adv. Funct. Mater.* **2014**, *24*, 151−157.
(15) Liu, D.; Kelly, T. L. Perovskite Solar Cells with a Planar Heterojunction Structure Prepared Using Room-Temperature Solution Processing Techniques. *Nat. Photonics* **2014**, *8*, 133−138.
(16) You, J.; et al. Low-Temperature Solution-Processed Perovskite Solar Cells with High Efficiency and Flexibility. *ACS Nano* **2014**, *8*, 1674−1680.
(17) Barrows, A. T.; Pearson, A. J.; Kwak, C. K.; Dunbar, A. D. F.; Buckley, A. R.; Lidzey, D. G. Efficient Planar Heterojunction Mixed-Halide Perovskite Solar Cells Deposited via Spray-Deposition. *Ener. Environ. Sci.* **2014**, *7*, 2944.
(18) Ball, J. M.; Lee, M. M.; Hey, A.; Snaith, H. J. Low-Temperature Processed Meso-Superstructured to Thin-Film Perovskite Solar Cells. *Ener. Environ. Sci.* **2013**, *6*, 1739−1743.
(19) He, M.; Zheng, D.; Wang, M.; Lin, C.; Lin, Z. High Efficiency Perovskite Solar Cells: From Complex Nanostructure to Planar Heterojunction. *J. Mater. Chem. A* **2014**, *2*, 5994−6003.
(20) Gratzel, M. The Light and Shade of Perovskite Solar Cells. *Nat. Mater.* **2014**, *13*, 838−42.
(21) Leijtens, T.; et al. Electronic Properties of Meso-Superstructured and Planar Organometal Halide Perovskite Films: Charge Trapping, Photodoping, and Carrier Mobility. *ACS Nano* **2014**, *8*, 7147−7155.
(22) Liu, M.; Johnston, M. B.; Snaith, H. J. Efficient Planar Heterojunction Perovskite Solar Cells by Vapour Deposition. *Nature* **2013**, *501*, 395−398.
(23) Chen, Q.; Zhou, H.; Hong, Z.; Luo, S.; Duan, H. S.; Wang, H. H.; Liu, Y.; Li, G.; Yang, Y. Planar Heterojunction Perovskite Solar Cells via Vapor-Assisted Solution Process. *J. Am. Chem. Soc.* **2014**, *136*, 622−625.
(24) Snaith, H. J.; et al. Anomalous Hysteresis in Perovskite Solar Cells. *J. Phys. Chem. Lett.* **2014**, *5*, 1511−1515.

DOI: 10.1021/jz502720a
J. Phys. Chem. Lett. 2015, 6, 493−499

(25) Unger, E. L.; Hoke, E. T.; Bailie, C. D.; Nguyen, W. H.; Bowring, A. R.; Heumuller, T.; Christoforo, M. G.; McGehee, M. D. Hysteresis and Transient Behavior in Current−Voltage Measurements of Hybrid-Perovskite Absorber Solar Cells. *Ener. Environ. Sci.* **2014**, *7*, 3690−3698.
(26) Stranks, S. D.; Eperon, G. E.; Grancini, G.; Menelaou, C.; Alcocer, M. J. P.; Leijtens, T.; Herz, L. M.; Petrozza, A.; Snaith, H. J. Electron-Hole Diffusion Lengths Exceeding 1 Micrometer in an Organometal Trihalide Perovskite Absorber. *Science* **2013**, *342*, 341−344.
(27) Colella, S.; et al. $MAPbI_{3-x}Cl_x$ Mixed Halide Perovskite for Hybrid Solar Cells: The Role of Chloride As Dopant on the Transport and Structural Properties. *Chem. Mater.* **2013**, *25*, 4613−4618.
(28) Unger, E. L.; et al. Chloride in Lead Chloride-Derived Organo-Metal Halides for Perovskite-Absorber Solar Cells. *Chem. Mater.* **2014**, *26*, 7158−7165.
(29) Dar, M. I.; Arora, N.; Gao, P.; Ahmad, S.; Grätzel, M.; Nazeeruddin, M. K. Investigation Regarding the Role of Chloride in Organic−Inorganic Halide Perovskites Obtained from Chloride Containing Precursors. *Nano Lett.* **2014**, *14*, 6991−6996.
(30) Williams, S. T.; Zuo, F.; Chueh, C.-C.; Liao, C.-Y.; Liang, P.-W.; Jen, A. K. Y. Role of Chloride in the Morphological Evolution of Organo-Lead Halide Perovskite Thin Films. *ACS Nano* **2014**, *8*, 10640−10654.
(31) Yu, H.; Wang, F.; Xie, F.; Li, W.; Chen, J.; Zhao, N. The Role of Chlorine in the Formation Process of "$CH_3NH_3PbI_{3-x}Cl_x$" Perovskite. *Adv. Funct. Mater.* **2014**, *24*, 7102−7108.
(32) Poglitsch, A.; Weber, D. Dynamic Disorder in Methylammoniumtrihalogenoplumbates (II) Observed by Millimeter-Wave Spectroscopy. *J. Chem. Phys.* **1987**, *87*, 6373−6378.
(33) Tidhar, Y.; Edri, E.; Weissman, H.; Zohar, D.; Hodes, G.; Cahen, D.; Rybtchinski, B.; Kirmayer, S. Crystallization of Methyl Ammonium Lead Halide Perovskites: Implications for Photovoltaic Applications. *J. Am. Chem. Soc.* **2014**, *136*, 13249−13256.
(34) Brixner, L. H.; Chen, H. Y.; Foris, C. M. X-ray Study of the $PbCl_{2-x}I_x$ and $PbBr_{2-x}I_x$ Systems. *J. Solid State Chem.* **1981**, *40*, 336−343.
(35) Chen, Q.; Zhou, H.; Song, T.-B.; Luo, S.; Hong, Z.; Duan, H.-S.; Dou, L.; Liu, Y.; Yang, Y. Controllable Self-Induced Passivation of Hybrid Lead Iodide Perovskites toward High Performance Solar Cells. *Nano Lett.* **2014**, *14*, 4158−4163.
(36) Buin, A.; Pietsch, P.; Xu, J.; Voznyy, O.; Ip, A. H.; Comin, R.; Sargent, E. H. Materials Processing Routes to Trap-Free Halide Perovskites. *Nano Lett.* **2014**, *14*, 6281−6286.
(37) De Wolf, S.; Holovsky, J.; Moon, S.-J.; Löper, P.; Niesen, B.; Ledinsky, M.; Haug, F.-J.; Yum, J.-H.; Ballif, C. Organometallic Halide Perovskites: Sharp Optical Absorption Edge and Its Relation to Photovoltaic Performance. *J. Phys. Chem. Lett.* **2014**, *5*, 1035−1039.
(38) Wehrenfennig, C.; Liu, M.; Snaith, H. J.; Johnston, M. B.; Herz, L. M. Homogeneous Emission Line Broadening in the Organo Lead Halide Perovskite $CH_3NH_3PbI_{3-x}Cl_x$. *J. Phys. Chem. Lett.* **2014**, *5*, 1300−1306.
(39) Xing, G.; Mathews, N.; Sun, S.; Lim, S. S.; Lam, Y. M.; Grätzel, M.; Mhaisalkar, S.; Sum, T. C. Long-Range Balanced Electron- and Hole-Transport Lengths in Organic−Inorganic $CH_3NH_3PbI_3$. *Science* **2013**, *342*, 344−347.
(40) Grancini, G.; et al. The Impact of the Crystallization Processes on the Structural and Optical Properties of Hybrid Perovskite Films for Photovoltaics. *J. Phys. Chem. Lett.* **2014**, 3836−3842.
(41) Docampo, P.; Hanusch, F. C.; Giesbrecht, N.; Angloher, P.; Ivanova, A.; Bein, T. Influence of the Orientation of Methylammonium Lead Iodide Perovskite Crystals on Solar Cell Performance. *APL Materials* **2014**, *2*, 081508.
(42) Agarwal, S.; Seetharaman, M.; Kumawat, N. K.; Subbiah, A. S.; Sarkar, S. K.; Kabra, D.; Namboothiry, M. A. G.; Nair, P. R. On the Uniqueness of Ideality Factor and Voltage Exponent of Perovskite-Based Solar Cells. *J. Phys. Chem. Lett.* **2014**, *5*, 4115−4121.

DOI: 10.1021/jz502720a
J. Phys. Chem. Lett. 2015, 6, 493−499